Journal of Molecular Structure 1271 (2023) 134100

Contents lists available at ScienceDirect

Journal of Molecular Structure

journal homepage: www.elsevier.com/locate/molstr

Co-doped zinc oxide nanoparticles embedded in Polyvinylalcohol Hydrogel as solar light derived photocatalyst disinfection and removal of coloured pollutants

Haya A. Abubshait[a,1], Muhammad Saad[b,1], Shahid Iqbal[b,*], Samar A. Abubshait[c], Ali Bahadur[d,*], Muhammad Raheel[e], Fwzah H. Alshammari[f], Norah Alwadai[g], Hamad Alrbyawi[h], Mohammed A.S. Abourehab[i,j], Eslam B. Elkaeed[k], Muhammad Abdul Qayyum[l], H.H. Somaily[m,n]

[a] Basic Sciences Department, Deanship of Preparatory Year and Supporting Studies, Imam Abdulrahman Bin Faisal University, P.O. Box 1982, Dammam 31441, Saudi Arabia
[b] Department of Chemistry, School of Natural Sciences (SNS), National University of Science and Technology (NUST), H-12, Islamabad 46000, Pakistan
[c] Department of Chemistry, College of Science, Imam Abdulrahman bin Faisal University, P.O. Box 1982, Dammam 31441, Saudi Arabia
[d] Department of Chemistry, College of Science and Technology Wenzhou-Kean University, Wenzhou, China
[e] Department of Chemistry, Balochistan University of Information Technology, Engineering and Management Sciences, Quetta, Pakistan
[f] Department of Physics, University Colleges at Nairiyah, University of Hafr Al Batin (UHB), Nairiyah 31981, Saudi Arabia
[g] Department of Physics, College of Sciences, Princess Nourah bint Abdulrahman University (PNU), Riyadh 11671, Saudi Arabia
[h] Pharmaceutics and Pharmaceutical Technology Department, College of Pharmacy, Taibah University, Medina Saudi Arabia
[i] Department of Pharmaceutics, College of Pharmacy, Umm Al-Qura University, Makkah 21955, Saudi Arabia
[j] Department of pharmaceutics and Industrial Pharmacy, Faculty of Pharmacy, Minia University, Minia 61519, Egypt
[k] Department of Pharmaceutical Sciences, College of Pharmacy, AlMaarefa University, Riyadh 13713, Saudi Arabia
[l] Department of Chemistry Division of Science and Technology University of Education Lahore Pakistan
[m] Research Center for Advanced Materials Science (RCAMS), King Khalid University, Abha 61413, P.O. Box 9004, Saudi Arabia
[n] Department of Physics, Faculty of Science, King Khalid University, P.O. Box 9004, Abha, Saudi Arabia

ARTICLE INFO

Article history:
Received 2 December 2021
Revised 3 September 2022
Accepted 5 September 2022
Available online 7 September 2022

Keywords:
ZnO nanoparticle
Polyvinyl alcohol
Photocatalyst
Solar light
Dye degradation
Disinfection

ABSTRACT

In this study Co doped ZnO NPs (CoZnO) were synthesized by using polyvinyl alcohol hydrogel (PVA HG) as platform for methyl orange dye (MO) degradation. CoZnO/PVA photocatalysts are not only effective to degrade organic pollutants but also used for disinfection the water. Co-doped zinc oxide nanoparticles (CoZnO NPs) as an excellent photocatalyst were synthesized by the coprecipitation method. ZnO NPs due to its large band gap is only UV light mediated photocatalyst which is only 4% of solar spectrum. In order to fully utilize of solar spectrum, low cast Co transition metal was doped to ZnO NPs to make is visible light derived photocatalyst by lowering its band gap. A high adsorption power of PVA HG enhance photocatalyst activity. For this purpose, Polyvinyl alcohol hydrogel was used along with Co doped ZnO NPs to enhance the photocatalytic activity. Polyvinyl alcohol hydrogel (PVA HG) was prepared by basic hydrolysis of polyvinyl acetate gel which was prepared by free radical emulsion method using diacrylate crosslinker. Co-doped ZnO NPs were formed in the PVA HG matrix by coprecipitation method. The doping concentration of Co was changed from 0-16%(w/w). and optimized for best photocatalytic ability. The 12% Co-doped ZnO NPs showed best photocatalytic ability. So, 12CoZnO NPs were incorporated in the PVAHG for dye degradation and disinfection study. The 12CoZnO/PVA yielded composite showed an extreme rise in photocatalytic efficiency and completely mineralized MO in 48 min. The prepared composite showed better degradation of methylene blue than 12CoZnO NPs under UV-vis light radiation. The stability of PVA/CoZnO NC for photodegradation of dye was verified by a recycling experiment of the composite.

1. Introduction

Photocatalysts are not only effective to degrade organic pollutants but also used for disinfection the water [1–3]. The photocatalyst generate reactive oxygen species which effectively kill the mi-

* Corresponding authors.
E-mail addresses: shahid.iqbal@hzu.edu.cn (S. Iqbal), abahadur@kean.edu (A. Bahadur).
[1] Authors contributed equally.

https://doi.org/10.1016/j.molstruc.2022.134100
0022-2860/

croorganisms. ZnO NPs can safely be used as medicine and antimicrobial agent [4–6]. ZnO is commonly used in sunscreens, because it effectively absorber the UV radiation due to wide bandgap [7–12]. The photocatalysts are also widely used to degrade the colored pollutant and wastewater treatment. Among the various type of photocatalysts, heterogeneous photocatalysts are more promising due to high potential in dye degradation and disinfection [8,13–17]. The efficiency of heterostructure photocatalyst can be enhance by doping of metals into semiconductor nanomaterials. Photocatalytic properties enhance many times when a heterostructure is formed between metal doped semiconductors and polymer materials, carbon materials, microgels, etc [18–22].

Generally, electron hole pair (e_{cb}^{-}-h_{vb}^{+}). $^{-}$ is produced in the photocatalytic reaction when photocatalyst is exposed to a suitable range of solar light which provide sufficient energy to transfer the electrons from valance band to conduction band of semiconductor photocatalyst [23–27]. These electron hole pair life is very short and recombine with the decapitation of heat which is the major drawback of photocatalyst efficiency [28–30]. These electron hole pairs can be trapped at the surface of photocatalyst with adsorbed pollutant which result degradation of organic pollutants by redox reaction. The recombination of electron hole pair can be reduced by doping and formation of nanocomposites which effectively delay the recombination of e-h pair. So, in this work, Co was doped into ZnO NPs to enhance its photocatalytic activity [31–34].

Wastewater containing colored impurities such as dyes and other water-soluble pollutants are difficult to remove from water by filtration [35–37]. Globally, a lot of environmental and ecological issues are associated with wastewater pollutants [38]. Each year, amount of colored pollutant discharged in wastewater increasing tremendously [39]. The existing physical, chemical, and biological methods for wastewater treatment are not efficient on large scale [40]. Photo catalytically degradation of pollutants with the help of photocatalyst in the presence of solar light is best method at the time which is cheap and ecofriendly [41–43]. For efficient photocatalyst system, the adsorbing material is very important and various materials such as different polymers, clay, carbon materials, and ceramics materials were used to enhance the adsorption of pollutants on the catalyst surface [44]. In this study Co doped ZnO NPs were synthesized by using polyvinyl alcohol hydrogel as platform for methyl blue dye degradation [45–47].

Photocatalysts are not only effective to degrade organic pollutants but also used for disinfection the water. These photocatalyst generate reactive oxygen species which effectively kill the microorganisms. ZnO NPs can safely be used as medicine and antimicrobial agent. ZnO is commonly used in sunscreens, because it effectively absorber the UV radiation due to wide bandgap. ZnO NPs due to its large band gap is only UV light mediated photocatalyst which is only 4% of solar spectrum. In order to fully utilize of solar spectrum, low cast Co transition metal was doped to ZnO nanoparticles to make is visible light derived photocatalyst by lowering its band gap. One important requirement of photocatalyst must have moderate adsorption of pollutants. A high adsorption power of photocatalyst enhance its activity and low adsorption ability makes its ineffective. For this purpose, Polyvinyl alcohol hydrogel was used along with Co doped ZnO NPs to enhance the photocatalytic activity. In this study, we have designed Co doped ZnO NPs then these NPs were incorporated into polyvinyl alcohol hydrogel. CoZnO photocatalyst was used to remove organic pollutants from wastewater and for disinfection purpose under visible light while polyvinyl alcohol hydrogel was used to enhance the adsorption of pollutant and stabilize the CoZnO NPs. The system was effectively sued for photo catalytically degradation of methyl blue dye and water disinfection. Co doped ZnO NPs were formed by co-precipitation method and polyvinyl alcohol hydrogel was synthesized by free radical polymerization method.

2. Materials and methods

2.1. Materials

All the analytical-grade reagents and solvents were acquired from Sigma-Aldrich and utilized directly. zinc acetate dihydrate ($Zn(CH_3COO)_2.2H_2O$, 98%, Sigma), cobalt acetate dihydrate ($Co(CH_3COO)_2.2H_2O$, 97%, E. Merk), ammonium persulfate (APS, 98.5%, Sigma), sodium hydroxide (NaOH, 99%, Sigma), methyl orange (MO, 98%, Sigma), de-ionized water and sodium lauryl sulfate were used in this study.

2.2. Synthesis of ZnO NP's

ZnO NPs were prepared by precipitation method. In the 1st step, $Zn(CH_3COO)_2.2H_2O$ (10.98 g, 50 mM) along with sodium lauryl sulfate (200 mg) was dissolved into distilled H_2O (100 mL) by stirring for 0.5 h. ZnO precipitates were formed by dropwise adding NaOH (4 M) until pH reached to 11 and heat for 0.5 h at 70 °C. ZnO NPs were filtered, washed with ethanol/H_2O repeatedly, and dried at room temperature overnight. The dried ZnO NPs were calcinated at 600 °C for 2 h in a muffle furnace. The calcinated ZnO NPs of the ZnO were grinded to a fine powder.

2.2.1. Preparation of polyvinyl alcohol hydrogel

Polyvinyl alcohol was synthesized by hydrolysis of polyvinyl acetate hydrogel. In first step polyvinyl acetate microgel was prepares by free radical emulsion polymerization using 1,4-butanediol diacrylate as crosslinker and ammonium persulfate as initiator. Briefly, water (200 mL), vinyl acetate monomer (10 mL), 1,4-butanediol diacrylate (1 ml), sodium lauryl sulfate (200 mg) and APS initiator (100 mg) were mixed ultrasonically and finally with high mechanical stirring. The resulting emulsion was heated at 65 °C in 500 mL round bottom flask under mechanical stirring for 4 h then at 70 °C for 30 min to get final polyvinyl acetate hydrogel

In second step, the polyvinyl acetate hydrogel was hydrolyzed under basic condition by using NaOH at pH 11 for 5 h. The final polyvinyl alcohol was obtained by precipitation in acetone and washed several times with acetone and water.

2.3. Preparation of co-doped ZnO NPs inside of polyvinyl alcohol hydrogel

Co doped ZnO NPs in the polyvinyl alcohol hydrogel were prepared by precipitation method as described in the synthesis of ZnO NPs section. In the 1st step, $Zn(CH_3COO)_2.2H_2O$ (10.98 g, 50 mM) and $Co(CH_3COO)_2.2H_2O$ with different doping amounts along with sodium lauryl sulfate (200 mg) was dissolved into distilled H_2O (100 mL) by stirring for 0.5 h. Then polyvinyl alcohol hydrogel (100 g) was soaked overnight in the Zn and Co precursor solution which was prepared in the previous step. Co doped ZnO precipitates inside the PVA were formed by dropwise adding NaOH (4 M) until pH reached to 11 and heat for 0.5 h at 70 °C. Co doped ZnO NPs were filtered, washed with ethanol/H_2O repeatedly, and dried at room temperature overnight. The dried Co doped ZnO NPs were calcinated at 600 °C for 2 h in a muffle furnace. The calcinated ZnO NPs of the ZnO were grinded to a fine powder.

3. Results and discussion

3.1. Structural properties

XRD was used to determine the crystal structures of the generated materials (Fig. 1). Using the usual hexagonal wurtzite structure of ZnO, all of the diffraction peaks in the XRD patterns of ZnO and CoZnO samples may be correctly indexed. It is probable that

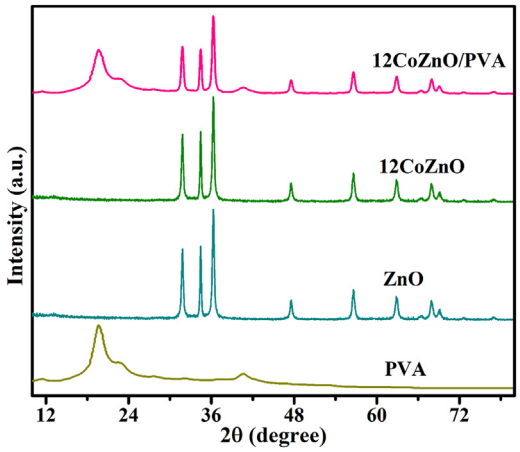

Fig. 1. XRD pattern of ZnO, 12CoZnO, Poly(vinyl alcohol) and 12CoZnO/PVA.

Co atoms have interstitially replaced Zn atoms in the hexagonal lattices since the XRD's sensitivity for cobalt doped samples was inadequate to detect the existence of CoO, Co_2O, or Co phases. This is a result of Zn^{2+}(0.73°A) ionic radius being close to Co^{2+}(0.70°A) ionic radius. Additionally, the principal peak of CoZnO samples exhibits a little shift toward a greater diffraction angle with increasing co-concentrations (Fig. 1). This change is due to the ionic radii of Co^{2+}(0.70°A) and Zn^{2+}(0.73°A), which vary from one another. The ensuing variance proved that the Co doping into the ZnO lattice was successful. 12CoZnO nanostructures and nanofilms have previously had similar explanations for this behaviour. In the XRD spectra of Poly(vinyl alcohol) microgel, a pronounced peak is produced at 19.59, which originates from past studies. The composite 12CoZnO/PVA material's XRD spectra, however, show distinct diffraction peaks for 2CoZnO and PVA. This result shows that the 12CoZnO was effectively absorbed into the PVA microgel.

In Fig. 2, the produced materials' TEM pictures are shown (a-d). The spherical, 18-28 nm sized ZnO NPs are shown in Fig. 2a. The 12CoZnO are also spherical, despite their small size (09-19 nm). However, equated to ZnO, the degree of aggregation of 12CoZnO NPs (Fig. 2b) is minimal. The PAV microgel that was created is translucent, semi-spherical in nature, and micrometers in size (Fig. 2c). The TEM profile of the composite demonstrated in Fig. 2d shows that the cross-linking among 12CoZnO and PVA microgels was effective. Fig. 2d makes it clear that the PVA microgel has evenly distributed and swallowed the 12CoZnO NPs, which have a diameter of 11 to 22 nm.

SEM-EDS microscopy was employed to analyse the surface morphology and fundamental components of ZnO, 12CoZnO, PVA, and 12CoZnO/PVA nanocomposites. The results are shown in Fig. 3 (a-h). Nanomaterials made of ZnO that have been produced are visible in SEM pictures as 3D floral structures. The incomplete nanosheets of ZnO that make up the "petals" of these flower-like morphologies (Fig. 3a) have a diameter in the micron range. The ZnO and 12CoZnO (Figs. 3b and 3d) showed the O, Zn elements and Co, O, Zn elements in the EDX spectrum, respectively, demonstrating the purity of these NPs. Instead of particles, the agglomerated nanoflakes make up the 12CoZnO NPs' morphology (Fig. 3c). In contrast to nanoflakes and particles, pure PVA has a translucent nanosheet-like structure (Fig. 3e), and its EDX spectrum exclusively exhibits C and O peaks (Fig. 3f), demonstrating the microgel's purity. Fig. 3g depicts the semispherical, somewhat agglomerated structure of the 12CoZnO/PVA NCs. Fig. 3g, a SEM image of 12CoZnO/PVA, shows how evenly distributed the 12CoZnO NPs are throughout the transparent network of Poly (vinyl alcohol) gel. Additionally, 12CoZnO/elemental PVA's composition (Fig. 3h) was ascertained using the EDX assessment, which established the composite's purity.

The results of the further XPS analysis of the chemical states and elemental arrangement of the constructed 12CoZnO/PVA NCs are shown in Fig. S1. Fig. 4a displays the FTIR measurements for the synthesized ZnO, 12CoZnO, PVA, and 12CoZnO/PVA NCs. Wideband are noticed in the FTIR measurements of ZnO and 12CoZnO at about 3298 cm^{-1} owing to -OH extending and at 1626 cm^{-1} due to -OH twisting. The bands about 1097 cm^{-1} are the result of the production of Zn-O-O-Zn (metal peroxide). Stretching of the Zn-O link causes the band at 593 cm^{-1}, which is caused by an increase in Co doping, to be moved to a higher frequency [48]. Therefore, FTIR spectra proved that ZnO and 12CoZnO were synthesized (Fig. 4a).

Peaks at 752 cm^{-1} correspond to the -CH_2 rocking mode in the FTIR spectra of PAV microgel and 12CoZnO/PVA NCs (Fig. 4a), however peaks at 1060 cm^{-1} belong to the C-CH_2 widening. The key peaks in the spectra of the PVA microgel and 12CoZnO/PVA NCs include the -CH_2 bending peak at 1441 cm^{-1}, the COO- peak at 1449 cm^{-1} (symmetric), the COO- stretching peak at 1570 cm^{-1} (antisymmetric), and the peak in 1711 cm1 which is caused by the free carboxyl group (COOH). The -OH group is responsible for the peaks at 2729 cm^{-1}, 2839 cm^{-1}, and 3429 cm^{-1}, which are caused by the CH- extending mode and the -NH stretching mode, respectively [49,50]. The peaks of 12CoZnO NPs have been obscured in the FTIR spectra of 12CoZnO/PVA NCs by Poly(vinyl alcohol) linkages.

To test the materials' capacity for photo-induced charge separation, PL spectroscopy, a commonly used technique, was used. Fig. 4b displays the PL spectra of the samples under consideration at a 415 nm excitation wavelength. The fact that ZnO emits in a recognizable band at around 396-408 nm is consistent with earlier findings. The redshift in 12CoZnO and 12CoZnO/PVA is caused by modifications to the electrical structure, the appearance of defects in the visible area, and a reduction in bandgap. Although the PL intensity was low compared to ZnO and 12CoZnO, the 12CoZnO NPs were introduced into the PVA microgel. Due to the homogeneous distribution of 12CoZnO in the PVA microgel and efficient charge transfer in the 12CoZnO/PVA NCs, the composite may have a lower PL intensity. Therefore, the conjugation of the PVA microgel with the 12CoZnO/PVA photocatalyst could successfully stop the e-h set recombination [51].

Fig. 4c shows the findings of the BET technique's evaluation of the surface area of the manufactured materials using the N_2 adsorption-desorption method. Comparing 12CoZnO/PVA to ZnO and 12CoZnO, a high surface area was found. It is generally agreed upon that larger surface areas result in more active sites and make it easier for the photocatalyst to absorb an increasing content of pollutants. As a result, 12CoZnO/PVA NCs exhibit the maximum photocatalytic degradation and dye adsorption when compared to other samples. For pure ZnO, 12CoZnO NPs, and 12CoZnO/PVA NCs, the computed specific surface areas are as high as 14.52, 25.61, and 53.71 m^2 g^{-1}, respectively.

To identify the light-harvesting and bandgap properties of the produced samples, Figs. 4d and S2 show the UV-vis diffuse reflectance spectra. Since the ZnO displayed an optical absorption band roughly around 389 nm, it may be concluded that these NPs have a significant bandgap of 3.21 eV and are not visible light active. The band gap of 12CoZnO NPs has decreased (Eg = 2.97 eV), which is consistent with a large increase in the absorption of visible light. Absorption toward a longer wavelength was brought on by the incorporation of 12CoZnO into the Poly(vinyl alcohol) system (redshift). In line with this, a further reduction in the bandgap of 12CoZnO/PVA in comparison to 12CoZnO NPs (Eg = 2.91 eV) is seen, allowing for greater visible-light absorption. [47,48]

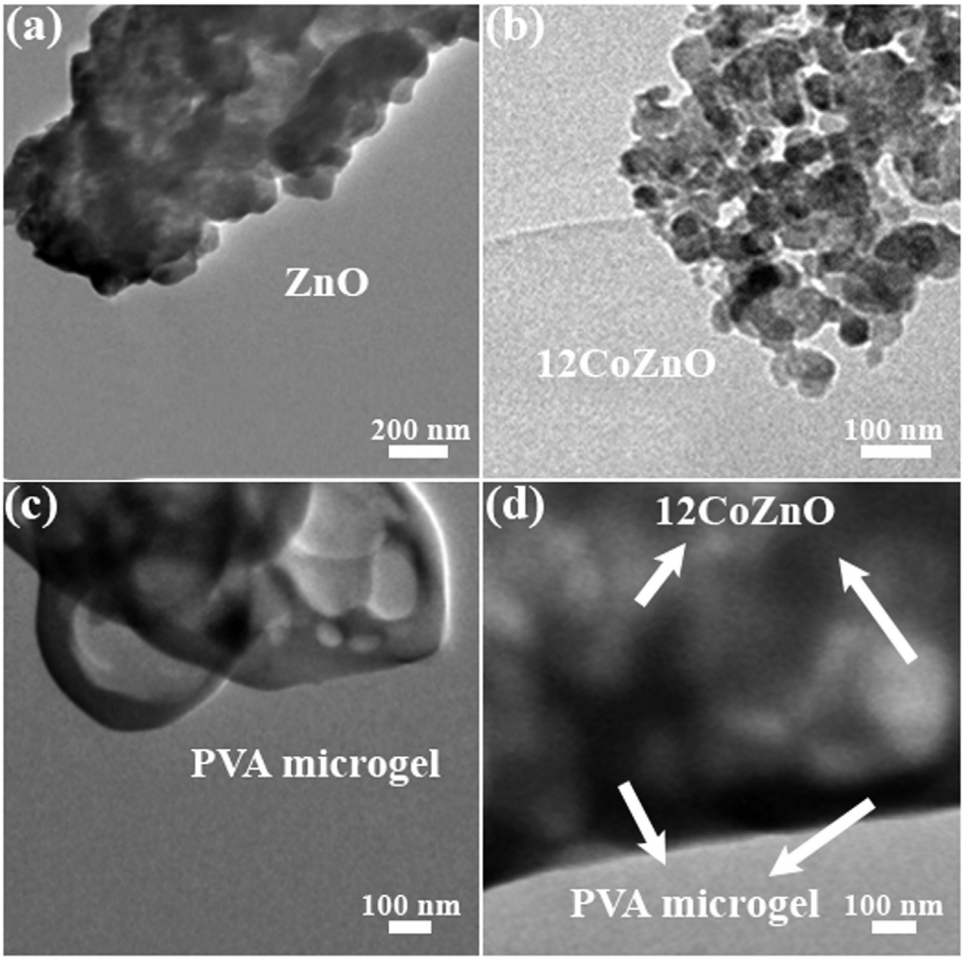

Fig. 2. TEM micrographs of (a) ZnO (b) 12CoZnO (c) PVA microgel and (d) 12CoZnO/PVA, respectively.

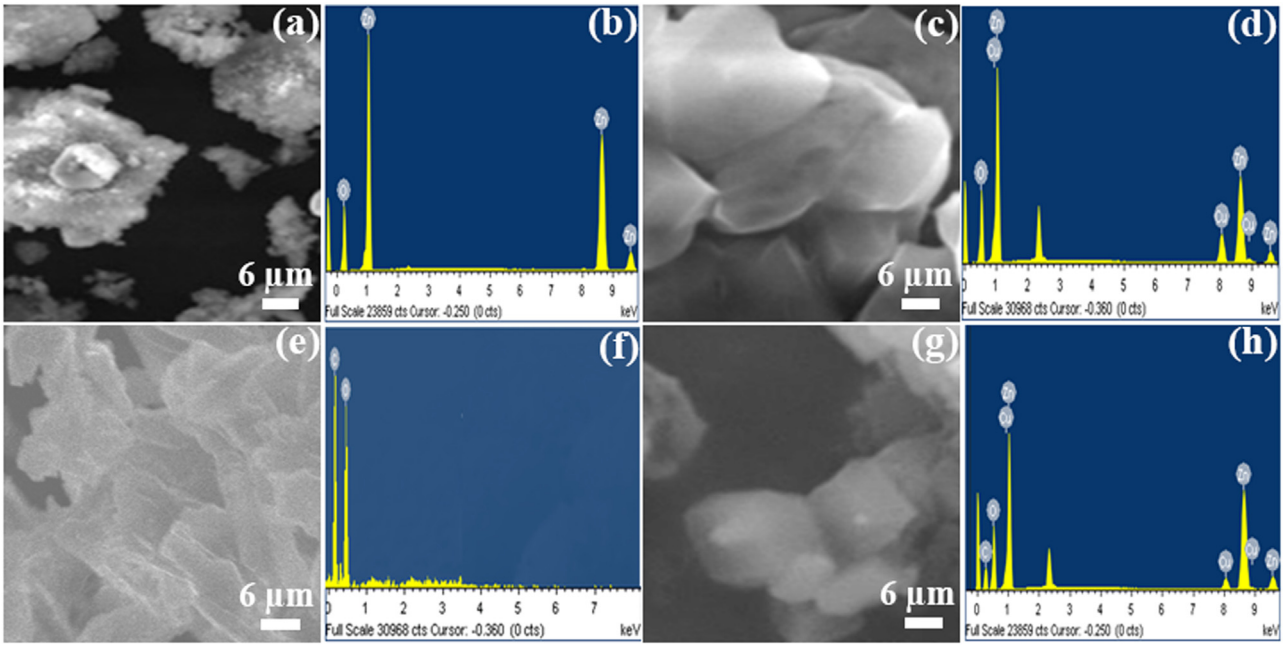

Fig. 3. SEM-EDX profiles of a, b ZnO, c, d 12CoZnO, e, f PVA, and g, h 12CoZnO/PVA.

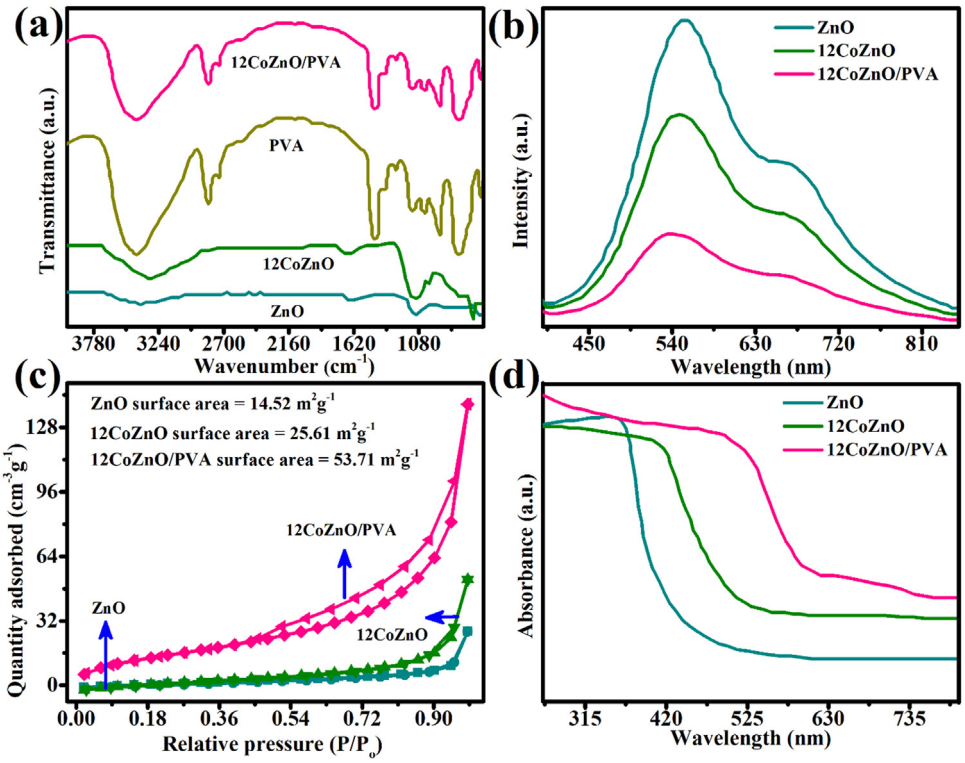

Fig. 4. (a) FTIR spectra of ZnO, 12CoZnO, PVA and 12CoZnO/PVA, (b) Photoluminescence spectra of ZnO, 12CoZnO and 12CoZnO/PVA, (c) surface area of ZnO, 12CoZnO and 12CoZnO/PVA and (d) UV-Vis diffuse reflectance spectra of ZnO, 12CoZnO and 12CoZnO/PVA, respectively.

3.2. The photocatalytic activity

Under the influence of sunlight, the photocatalytic degradation of MO by ZnO, CoZnO (4, 8, 12 and 16 wt.%), PVA and 12CoZnO/PVA samples was investigated. Figs. 5a and 5b show the rates of MO degradation by CoZnO and the resultant percentage degradation, 12CoZnO/PVA. Before the light was turned on, each sample had 35 min to attain adsorption-desorption equilibrium with the dye (4, 8, 12 and 16 wt. percent CoZnO). Compared to their contemporaries, the adsorption of the 12CoZnO NPs was at its highest. After achieving equilibrium, the NPs solutions in MO were exposed to sunshine. Fig. 5c displays the rates of MO deterioration. It is clear from Figs. 5a and 5c that 12CoZnO NPs outperformed other ZnO and CoZnO NPs in terms of photocatalysis and destroyed 85% of the MO in 112 min.

It's possible that the higher photocatalytic activity of 12CoZnO NPs is caused by Co doping, which results in more entrapping sites (defects) in the ZnO. These flaws reduce the rate of e^- and h^+ sets recombination and increase lifespan. The dye that has been adsorbed is subsequently destroyed by the charge carriers when they reach the photocatalyst surface [52,53]. The 12CoZnO NPs have a smaller energy bandgap than ZnO. The lower energy band gap also contributes to 12CoZnO's superior photocatalytic performance over ZnO. When a photon with energy equal to or greater than the photocatalyst's band gap is absorbed, an electron/hole pair is produced. So, changing the wavelength also changes the activity of the photocatalyst.

The photocatalytic efficiency of the 12CoZnO/PVA NCs was then assessed against MO in comparison to samples of ZnO, 12CoZnO NPs, and pure PVA. Afterward, 12CoZnO NPs and PVA were mixed to generate this material. The 12CoZnO/PVA NCs showed enriched photocatalytic proficiency in equated to ZnO, 12CoZnO, and PVA photocatalytic practices (Fig. 5d). The enhanced photocatalytic efficacy of 12CoZnO/PVA NCs may be attached to the equivalently distributed 12CoZnO in the PVA system (Fig. 5d). The incorporation of 12CoZnO into the PVA system resulted in quick charge passage through the PVA system, which successfully prevented the recombination of e-h couples. Because of their strong affinity for organic pollutants, the dye molecules are further adsorbate in the PVA microgel system, where they are subsequently destroyed by the 12CoZnO photocatalyst present in the NCs [55].

The 12CoZnO/PVA NCs mineralize MO to 98 percent of its original state in 48 min when exposed to sunshine (Fig. 5d). These findings suggest that the MO degradation process was effectively enhanced by the insertion of 12CoZnO NCs into the PVA microgel. As a result, 12CoZnO/PVA NCs have strong photocatalytic activity. The pseudo-first-order kinetics governs the photocatalytic dye degradation when exposed to solar light, and the rate constant was determined using the rate law.

$$ln\left(\frac{C_o}{C}\right) = kt$$

Where Co is the starting dye concentration, C is the dye concentration at any time (t), and k is the rate constant, respectively (Fig. 5d). In terms of MO degradation, the 12CoZnO/PVA NC has a higher k value (0.025 min^{-1}) than ZnO (0.0125 min^{-1}) and 12CoZnO (0.0150 min^{-1}). Here, we demonstrate that dye degradation occurs somewhat more quickly (48 min.) than in previous research (Table 1). [35,54]. According on BET research, 12CoZnO/PVA NCs had the most surface area when equated to other manufactured samples (Fig. 4c). The 12CoZnO/PVA NCs' significant improvement in photocatalytic performance may be attributed to their large specific surface area (53.71 m^2 g^{-1}) and quick charge transfer between the PVA microgel system and 12CoZnO interface. Importantly, it was shown that 12CoZnO/PVA NCs were the greatest photocatalyst, and they were subsequently employed in the recycling experiment.

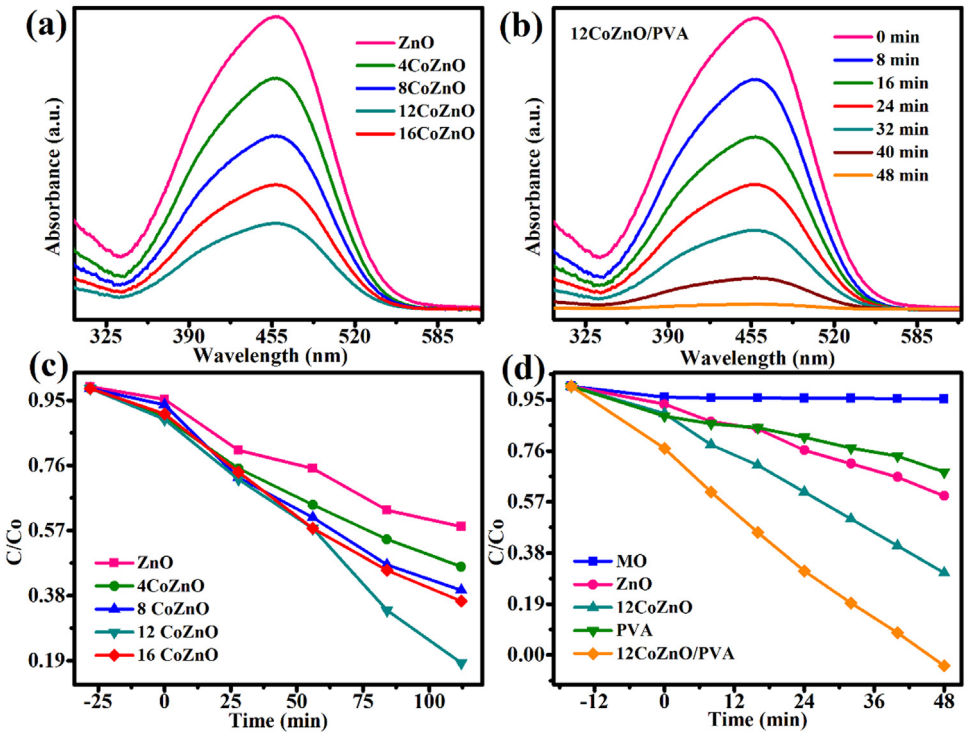

Fig. 5. Photocatalytic mineralization rate of MO by (a), (c) undoped and cobalt doped ZnO and (b) 12CoZnO/PVA. (d) Pseudo- first-order kinetic plots of MO, ZnO, 12CoZnO, PVA and 12CoZnO/PVA.

Table 1
Comparison of the 12CoZnO/PVA NCs' photocatalytic efficiency with certain earlier investigations.

Sr. No	Catalyst	Dye	Light Source	Irradiation Time (min.)	Degradation %	Ref.
1	ZnO	CV	UV	400	95	[55]
2	Ni-ZnO-p(AAc)	MB	Solar	60	95	[56]
3	ZnO-In_2O_3	MO	Solar	60	100	[57]
4	CeO_2-CuO	MB	Solar	300	80	[58]
5	12CoZnO/PVA	MO	Solar	60	100	Present study

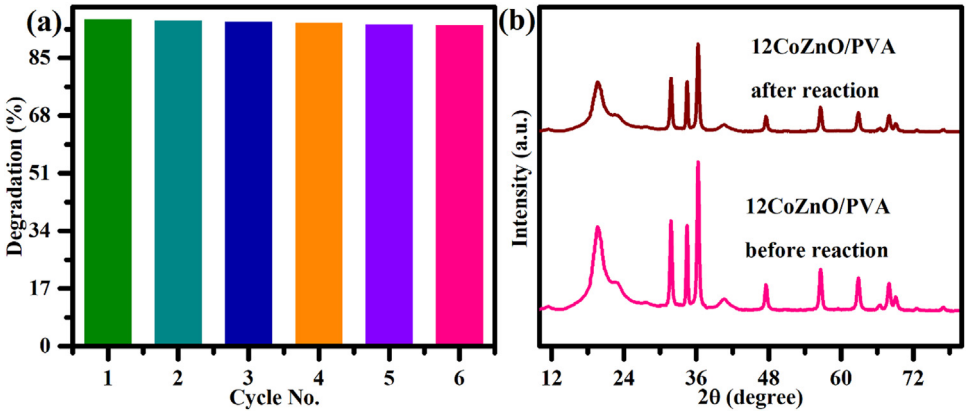

Fig. 6. (a) The 12CoZnO/PVA photocatalysts' cyclic stability up to the sixth cycle and (b) By comparing XRD patterns taken before the first cycle and after the sixth recycling experiment, structural stability of 12CoZnO/PVA was discovered.

3.3. Reusability of composite catalysts

By degrading MO six times progressively, the stability of the 12CoZnO/PVA NCs was examined. The obtained results demonstrated efficient MO decomposition and maintained over 90% even after the sixth recycling (Fig. 6a). Nevertheless, the catalytic rates rapidly declined after the 1st cycle. The slight decline in catalytic efficiency might be attributed to the partial blocking of active sites. As a result, the 12CoZnO/PVA catalysts could work as efficient, dependable, and reusable NCs. The XRD patterns of 12CoZnO/PVA NCs from the first and sixth cycles of dye photodegradation evaluations are shown in Fig. 6b, respectively. According to the stability

Table 2
Bactericidal efficiency of ZnO, 12CoZnO, and 12CoZnO/PVA NCs.

Antimicrobial agent	Escherichia Coli (mm)	Bacillus subtilis (mm)	Streptococcus salivarius (mm)	Staphylococcus aureus (mm)
Positive control	18	19	22	17
ZnO	6.9	4.8	7.4	6.5
12CoZnO	10.5	9.8	12.7	11.6
12CoZnO/PVA	20.4	15.7	21.7	20.4

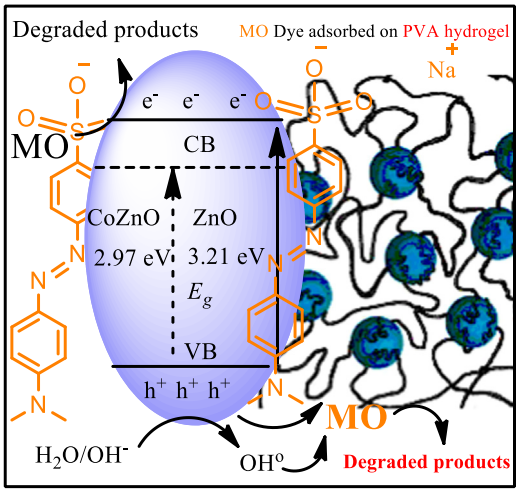

Fig. 7. The suggested mechanism for MO photocatalytic degradation using 12CoZnO/PVA composite.

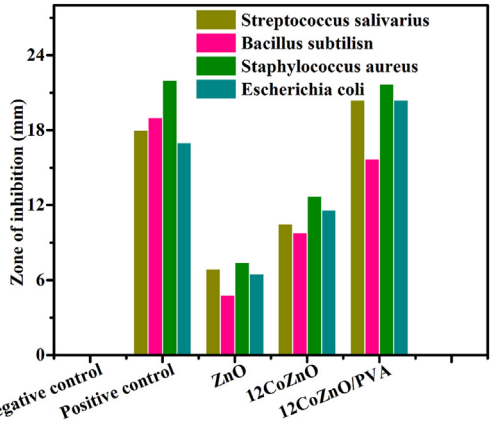

Fig. 8. Zones of inhibition of the ZnO, 12CoZnO NPs, and 12CoZnO/PVA against the used bacterial strains.

study, there were no discernible changes in the crystal phase structure of the 12CoZnO/PVA NCs before or after the organic pollutants recycling studies, indicating chemical structural resilience.

The manufactured NCs' photocatalytic mechanism under sunshine is described in Fig. 7. XRD patterns taken before the first cycle and after the sixth recycling experiment revealed the structural integrity of 12CoZnO/PVA. ROS (O^-_2, $^\bullet$OH and $^\bullet$OOH) are formed when the photogenerated e^- and h^+ sets interact with the oxygen and H_2O chemisorbed on the composite [59]. These ROS sparked a series of oxidation cases that efficiently mineralized the densely adsorbed and entrapped MO molecules in the microgel assembly. On 12CoZnO/PVA catalysts, the photocatalytic destruction of MO (organic pollutants) may be triggered by the transfer of holes or by •OH radicals.

Additionally, the created holes may yield •OH radicals and directly oxidise MO [60]. In comparison to PVA and 12CoZnO NPs, the 12CoZnO/PVA NCs exhibit more photoactive sites for pollutant degradation [61]. Therefore, the chemical interaction between PVA and 12CoZnO may be accountable for the enhanced photocatalytic performance of the 12CoZnO/PVA NCs. The distinctive PVA microgel structure prevents the ZnO photo-corrosion from occurring while the dye is being degraded by light. As a result, the 12CoZnO/PVA NCs are excellent candidates for use in photocatalytic decontamination of environmental organic contaminants.

3.4. Antibacterial study

Gram-positive and Gram-negative classes of bacteria were subjected to the antibacterial activity of the ZnO, 12CoZnO, and 12CoZnO/PVA NCs. Using the common ager diffusion methodology, the antibacterial activity was carried out. The antibacterial testing was conducted against four distinct bacterial strains: Staphylococcus aureus, Bacillus subtilis, Escherichia coli, and Streptococcus salivarius. The Petri dishes were removed and positioned under a laminar flow hood after the incubation time. Table 2 contains the measurements and records of the zones of inhibition for each sample, including the positive and negative controls. The zones of inhibition for each nanomaterial against each of the four bacterial strains were measured and recorded using the same process.

It was discovered that all four bacterial strains had a zone of suppression when exposed to the nanomaterials ZnO, 12CoZnO NPs, and 12CoZnO/PVA NCs. The 12CoZnO/PVA NCs has the highest bacterial inhibition zones, while ZnO had the lowest. The maximum antibacterial activity of the 12CoZnO/PVA NCs may have resulted from the enhanced formation of ROS caused by the narrowing of the ZnO bandgap and the high surface area given by 12CoZnO NPs for surface contact NCs with bacterial membrane. All generated samples were examined for zones of inhibition against the four bacterial strains shown in Fig. 8 below. The ternary composite exhibits superior antibacterial activity than the other synthetic nanomaterials, as seen in the bar graph below.

4. Conclusions

Among different Co-doped ZnO NPs, 12% Co doped ZnO NPs showed best photocatalytic activity and degraded 85% the dye within 112 min. 12% CoZnO NPs incorporated PVA HG degraded the dye (98%) within 48 min. The size of CoZnO NPs were in the range of 30-50 nm and uniformly distributed in PVAHG as confirmed by SEM and TEM images. The high antibacterial activity and photocatalytic ability of 12% CoZnO NPs composite in PVAHG was due to moderate adsorption ability of hydrogel and high surface area. The 12CoZnO/PVA NCs has the highest bacterial inhibition zones, while ZnO NPs had the lowest.

Credit Author Statement

Haya A. Abubshait: Conception, performed photocatalytic experiments, visualization of data, writing reviewing, and editing. **Muhammad Saad:** Conducted SEM analysis, performed FTIR analysis, interpretation of data, writing-original draft preparation. **Shahid Iqbal:** Design of study, performed major experimental works, writing-original draft preparation. **Samar A. Abubshait:**

Material synthesis, visualization of data, writing reviewing, and editing. **Ali Bahadur:** Methodology, reviewed original manuscript, and critical revision. **Muhammad Raheel:** Conducted XRD analysis, acquisition of data, writing-original draft preparation. **Fwzah H. Alshammari:** Analysis and/or interpretation of data, performed FTIR analysis. **Norah Alwadai:** Conception, design of study, writing-original draft preparation and critical revision, supervision. **Hamad Alrbyawi:** Drafting the revised manuscript, performed XRD analysis and critical revision. **Mohammed A.S. Abourehab:** Conception, design of the study, acquisition of data, interpret the data. **Eslam B. Elkaeed:** Visualization of data, reviewed the original manuscript and critical revision. **Muhammad Abdul Qayyum:** Reviewed original manuscript, and critical revision. **H.H. Somaily:** Reviewed original manuscript, and critical revision.

Declaration of Competing Interest

The authors declare no conflict of interest.

Data availability

Data will be made available on request.

Acknowledgment

This work was supported by King Khalid University through a grant (KKU/RCAMS/22) under the Research Center for Advanced Materials Science (RCAMS) at King Khalid University, Saudi Arabia. “The authors would like to thank the Deanship of Scientific Research at Umm Al-Qura University for supporting this work by Grant Code: (22UQU4290565DSR71). Email: maabourehab@uqu.edu.sa”.

Supplementary materials

Supplementary material associated with this article can be found, in the online version, at doi:10.1016/j.molstruc.2022.134100.

References

[1] X. Yang, S. Sun, L. Ye, D. Yun, C. Liu, Y. Guo, B. Yang, M. Yang, Q. Yang, S. Liang, J. Cui, One-pot integration of S-doped BiOCl and ZnO into type-II photocatalysts: Simultaneously boosting bulk and surface charge separation for enhanced antibiotic removal, Sep. Purif. Technol. 299 (2022) 121725.
[2] M. Guo, W. Jiang, J. Ding, J. Lu, Highly active and recyclable CuO/ZnO as photocatalyst for transesterification of waste cooking oil to biodiesel and the kinetics, Fuel 315 (2022) 123254.
[3] I. Ahmad, S. Shukrullah, M.Y. Naz, H.N. Bhatti, M. Ahmad, E. Ahmed, S. Ullah, M. Hussien, Recent progress in rare earth oxides and carbonaceous materials modified ZnO heterogeneous photocatalysts for environmental and energy applications, J. Environ. Chem. Eng. 10 (2022) 107762.
[4] R. Liu, D. Zuo, C. Tan, Construction of C/ZnO/BiOI photocatalyst for enhanced degradation of carbaryl: characterization, performance and mechanism, J. Alloys Compd. 911 (2022) 165023.
[5] C. Zang, X. Han, H. Chen, H. Zhang, Y. Lei, H. Liu, C. Wang, G. Zhang, M. Ge, In situ growth of ZnO/Ag2O heterostructures on PVDF nanofibers as efficient visible-light-driven photocatalysts, Ceram. Int. 48 (2022) 27379–27387.
[6] S. Iqbal, Spatial charge separation and transfer in L-cysteine capped NiCoP/CdS nano-heterojunction activated with intimate covalent bonding for high-quantum-yield photocatalytic hydrogen evolution, 274 (2020) 119097.
[7] I. Ahmad, S. Shukrullah, M.Y. Naz, E. Ahmed, M. Ahmad, Rare earth metals co-doped ZnO/CNTs composite as high performance photocatalyst for hydrogen production from water_triethanolmine mixture, Int. J. Hydrogen Energy 47 (2022) 9283–9294.
[8] M. Ghorbani, A.R. Solaimany Nazar, M. Frahadian, M. Khosravi, Facile synthesis of Z-scheme ZnO-nanorod @ BiOBr-nanosheet heterojunction as efficient visible-light responsive photocatalyst: the effect of electrolyte and scavengers, J. Photochem. Photobiol. A 429 (2022) 113930.
[9] S. Iqbal, M. Javed, A. Bahadur, M.A. Qamar, M. Ahmad, M. Shoaib, M. Raheel, N. Ahmad, M.B. Akbar, H. Li, Journal of Materials Science: Materials in Electronics, Controlled synthesis of Ag-doped CuO nanoparticles as a core with poly (acrylic acid) microgel shell for efficient removal of methylene blue under visible light, 31 (2020) 8423-8435.
[10] T. Sindhu, R. Pavithran, A. Vidhya, Design of 3D-supramolecular metal organic framework of zinc as photocatalyst for the degradation of methylene blue through advanced oxidation process, Journal of Molecular Structure. 1245 (2021) 131039.
[11] S. Kumar, K.R. Reddy, C. Reddy, N.P. Shetti, V. Sadhu, M. Shankar, V.G. Reddy, A. Raghu, T.M. Aminabhavi, Metal nitrides and graphitic carbon nitrides as novel photocatalysts for hydrogen production and environmental remediation, in: Nanostruct. Mater. Environ. Appl., Springer, 2021, pp. 485–519.
[12] K.R. Reddy, M. Jyothi, A. Raghu, V. Sadhu, S. Naveen, T.M. Aminabhavi, Nanocarbons-supported and polymers-supported titanium dioxide nanostructures as efficient photocatalysts for remediation of contaminated wastewater and hydrogen production, in: Nanophotocatalysis and Environmental Applications, Springer, 2020, pp. 139–169.
[13] S. Iqbal, A. Bahadur, S. Anwer, S. Ali, R.M. Irfan, H. Li, M. Shoaib, M. Raheel, T.A. Anjum, M.J.C. Zulqarnain, S.A. Physicochemical, E. Aspects, Effect of temperature and reaction time on the morphology of L-cysteine surface capped chalcocite (Cu2S) snowflakes dendrites nanoleaves and photodegradation study of methyl orange dye under visible light, 601 (2020) 124984.
[14] M. Shalahuddin Al Ja’farawy, A.Purwanto Kusumandari, H. Widiyandari, Carbon quantum dots supported zinc oxide (ZnO/CQDs) efficient photocatalyst for organic pollutant degradation—a systematic review, Environ. Nanotechnol. Monit. Manag. 18 (2022) 100681.
[15] K.R. Reddy, B. Hemavathi, G.R. Balakrishna, A. Raghu, S. Naveen, M. Shankar, Organic conjugated polymer-based functional nanohybrids: synthesis methods, mechanisms and its applications in electrochemical energy storage supercapacitors and solar cells, in: Polymer Composites with Functionalized Nanoparticles, Elsevier, 2019, pp. 357–379.
[16] M. Jyothi, V. Nayak, K.R. Reddy, S. Naveen, A. Raghu, Non-metal (oxygen, sulphur, nitrogen, boron and phosphorus)-doped metal oxide hybrid nanostructures as highly efficient photocatalysts for water treatment and hydrogen generation, in: Nanophotocatalysis and Environmental Applications, Springer, 2019, pp. 83–105.
[17] J.L. Hodala, D.J. Moon, K.R. Reddy, C.V. Reddy, T.N. Kumar, M.I. Ahamed, A.V. International Journal of Hydrogen Energy Raghu, Catalyst design for maximizing C5+ yields during Fischer–Tropsch synthesis, 46 (2021) 3289-3301.
[18] S. Iqbal, M. Javed, M.A. Qamar, A. Bahadur, M. Fayyaz, A. Akbar, H.O. Alsaab, N.S. Awwad, H.A. Ibrahium, Synthesis of Cu-ZnO/polyacrylic acid hydrogel as visible-light-driven photocatalyst for organic pollutant degradation, 7 (2022) e202103694.
[19] C. Kuang, P. Tan, A. Bahadur, S. Iqbal, M. Javed, M.A. Qamar, M. Fayyaz, G. Liu, O.M. Alzahrani, E. Alzahrani, A.-E. Farouk, Dye degradation study by incorporating Cu-doped ZnO photocatalyst into polyacrylamide microgel, J. Mater. Sci. Mater. Electron. (2022).
[20] A. Bahadur, A. Saeed, M. Shoaib, S. Iqbal, S. journal of applied polymer science Anwer, Modulating the burst drug release effect of waterborne polyurethane matrix by modifying with polymethylmethacrylate, 136 (2019) 47253.
[21] L. Wang, H. Xu, J. Gao, J. Yao, Q. Zhang, Recent progress in metal-organic frameworks-based hydrogels and aerogels and their applications, Coord. Chem. Rev. 398 (2019) 213016.
[22] C. Li, H. Xu, J. Gao, W. Du, L. Shangguan, X. Zhang, R.-B. Lin, H. Wu, W. Zhou, X. Liu, J. Yao, B. Chen, Tunable titanium metal–organic frameworks with infinite 1D Ti–O rods for efficient visible-light-driven photocatalytic H_2 evolution, 7 (2019) 11928-11933.
[23] R. Muhammad Irfan, M. Hussain Tahir, M. Maqsood, Y. Lin, T. Bashir, S. Iqbal, J. Zhao, L. Gao, M. Haroon, CoSe as non-noble-metal cocatalyst integrated with heterojunction photosensitizer for inexpensive H2 production under visible light, J. Catal. (2020).
[24] E.T. Wahyuni, N.P. Diantariani, I. Kartini, A. Kuncaka, Enhancement of the photostability and visible photoactivity of ZnO photocatalyst used for reduction of Cr(VI) ions, Results Eng. 13 (2022) 100351.
[25] M. Rahal, Y. Atassi, I. Alghoraibi, Preparation of separable MnFe2O4/ZnO/CQDs as a visible light photocatalyst for Gentamicin treatment, Mater. Chem. Phys. 286 (2022) 126123.
[26] Y. Yan, C. Li, Y. Wu, J. Gao, Q. Journal of Materials Chemistry A, From isolated Ti-oxo clusters to infinite Ti-oxo chains and sheets: recent advances in photoactive Ti-based MOFs, 8 (2020) 15245-15270.
[27] Y. Yan, C. Li, Y. Wu, J. Gao, Q. Zhang, From isolated Ti-oxo clusters to infinite Ti-oxo chains and sheets: recent advances in photoactive Ti-based MOFs, J. Mater. Chem. A 8 (2020) 15245–15270.
[28] K. Ayeb, N. Moussa, G. Marcì, E.I. García-López, M.F. Nsib, L. Palmisano, Synergetic effect of oxygen vacancies and morphology of ZnO photocatalyst prepared by non-hydrolytic sol-gel route for the photo-oxidation of 2-propanol in a gas-solid system, Surf. Interfaces 32 (2022) 102162.
[29] M. Habibi, A. Habibi-Yangjeh, S.R. Pouran, C. Xu, C. Wang, Binary visible–light-triggered ZnO/Bi4O5Br2 photocatalysts with n-n heterojunction: simple fabrication and impressively activation of peroxodisulfate ions for degradation of tetracycline, Surf. Interfaces 32 (2022) 102147.
[30] F.F. Alharbi, S. Manzoor, T. Munawar, M.U. Nisa, A.G. Abid, F. Iqbal, S. Aman, M.F. Ehsan, M. Najam-Ul-Haq, M.N. Ashiq, Sunlight activated S-scheme ZnO–CoTe binary photocatalyst for effective degradation of dye pollutants from wastewater, Surf. Interfaces 31 (2022) 101991.
[31] M. Faisal, M.A. Rashed, J. Ahmed, M. Alsaiari, A.S. Alkorbi, M. Jalalah, S.A. Alsareii, F.A. Harraz, Rapid photodegradation of linezolid antibiotic and methylene blue dye over Pt nanoparticles/polypyrrole-carbon black/ZnO novel visible light photocatalyst, J. Environ. Chem. Eng. 9 (2021) 106773.

[32] J.-T. Lee, S.-W. Lee, M.-Y. Wey, S-scheme g-C3N4/ZnO heterojunction photocatalyst with enhanced photodegradation of azo dye, J. Taiwan Inst. Chem. Eng. 134 (2022) 104357.
[33] M. Shoaib, A. Bahadur, M.S. ur Rahman, S. Iqbal, M.I. Arshad, M.A. Tahir, T. Mahmood, Technology, sustained drug delivery of doxorubicin as a function of pH, releasing media, and NCO contents in polyurethane urea elastomers, Journal of Drug Delivery Science and Technology 39 (2017) 277-282.
[34] J. Zhang, M. Kuang, Y. Cao, Z. Ji, Environment-friendly ternary ZnO/ZnFe2O4/TiO2 composite photocatalyst with synergistic enhanced photocatalytic activity under visible-light irradiation, Solid State Sci. 129 (2022) 106913.
[35] T. Sansenya, N. Masri, T. Chankhanittha, T. Senasu, J. Piriyanon, S. Mukdasai, S. Nanan, Hydrothermal synthesis of ZnO photocatalyst for detoxification of anionic azo dyes and antibiotic, J. Phys. Chem. Solids 160 (2022) 110353.
[36] Z. Tang, F. Zhu, J. Zhou, W. Chen, K. Wang, M. Liu, N. Wang, N. Li, Monolithic NF@ZnO/Au@ZIF-8 photocatalyst with strong photo-thermal-magnetic coupling and selective-breathing effects for boosted conversion of CO2 to CH4, Appl. Catal. B 309 (2022) 121267.
[37] A. Bahadur, M. Shoaib, S. Iqbal, A. Saeed, M.S. ur Rahman, P.A. Channar, Polymers, Regulating the anticancer drug release rate by controlling the composition of waterborne polyurethane, Reactive and Functional Polymers 131 (2018) 134-141.
[38] S. Gea, S.A. Situmorang, N. Pasaribu, A.F.R. Piliang, B. Attaurrazaq, R.M. Sari, K.M. Pasaribu, S. Goutianos, Facile synthesis of ZnO–Ag nanocomposite supported by graphene oxide with stabilised band-gap and wider visible-light region for photocatalyst application, J. Mater. Res. Technol. 19 (2022) 2730–2741.
[39] S. Anwer, D.H. Anjum, S. Luo, Y. Abbas, B. Li, S. Iqbal, K. Liao, 2D Ti3C2Tx MXene nanosheets coated cellulose fibers based 3D nanostructures for efficient water desalination, Chem. Eng. J. 406 (2021) 126827.
[40] A. Bahadur, S. Iqbal, H.O. Alsaab, N.S. Awwad, H.A. Ibrahium, Designing a novel visible-light-driven heterostructure Ni–ZnO/S-g-C_3N_4 photocatalyst for coloured pollutant degradation, RSC Advances 11 (2021) 36518-36527.
[41] S. Iqbal, M. Javed, M.A. Qamar, A. Bahadur, M. Fayyaz, A. Akbar, H.O. Alsaab, N.S. Awwad, H.A. Ibrahium, Synthesis of Cu-ZnO/polyacrylic acid hydrogel as visible-light-driven photocatalyst for organic pollutant degradation, 7 (2022) e202103694.
[42] K. Riaz, S. Nadeem, A. Chrouda, S. Iqbal, A. Mohyuddin, S.U. Hassan, M. Javed, A. BaQais, N. Tamam, K. Aroosh, A. Rauf, M.A.S. Abourehab, M.I. Jamil, E.B. Elkaeed, R.M. Alzhrani, N.S. Awwad, H.A. Ibrahium, Coupling of Se-ZnFe2O4 with rGO for spatially charged separated nanocomposites as an efficient photocatalyst for degradation of organic pollutants in natural sunlight, Colloids Surf. A 649 (2022) 129332.
[43] A. Shawky, S.M. Albukhari, Design of Ag3VO4/ZnO nanocrystals as visible–light-active photocatalyst for efficient and rapid oxidation of ciprofloxacin antibiotic waste, J. Taiwan Inst. Chem. Eng. 133 (2022) 104268.
[44] M.W. Kadi, S.I. El-Hout, A. Shawky, R.M. Mohamed, Enhanced mercuric ions reduction over mesoporous S-scheme LaFeO3/ZnO p-n heterojunction photocatalysts, J. Taiwan Inst. Chem. Eng. 138 (2022) 104476.
[45] T. Chankhanittha, N. Komchoo, T. Senasu, J. Piriyanon, S. Youngme, K. Hemavibool, S. Nanan, Silver decorated ZnO photocatalyst for effective removal of reactive red azo dye and ofloxacin antibiotic under solar light irradiation, Colloids Surf. A 626 (2021) 127034.
[46] P. Molaei, F. Rahimi Moghadam, Seed-free synthesis of ZnO nanorods through egg white/glycerol medium for photocatalyst applications, Mater. Today Commun. 31 (2022) 103677.
[47] M. Javed, M.A. Qamar, S. Iqbal, S.O. Aljazzar, S. Iqbal, H. Khan, M.A.S. Abourehab, E.B. Elkaeed, A.I. Alharthi, N.S. Awwad, H.A. Ibrahium, Synergistic influences of doping techniques and well-defined heterointerface formation to improve the photocatalytic ability of the S-ZnO/GO nanocomposite, 7 (2022) e202201913.
[48] M. Navaneethan, G.K. Mani, S. Ponnusamy, K. Tsuchiya, C. Muthamizhchelvan, S. Kawasaki, Y. Hayakawa, Influence of Al doping on the structural, morphological, optical, and gas sensing properties of ZnO nanorods, J. Alloys Compd. 698 (2017) 555–564.
[49] L.J. Kirwan, P.D. Fawell, W.J.L. van Bronswijk, In situ FTIR-ATR examination of poly (acrylic acid) adsorbed onto hematite at low pH, 19 (2003) 5802-5807.
[50] K. Karthik, A. Raghu, K.R. Reddy, R. Ravishankar, M. Sangeeta, N.P. Shetti, C.V. Reddy, Green synthesis of Cu-doped ZnO nanoparticles and its application for the photocatalytic degradation of hazardous organic pollutants, Chemosphere 287 (2022) 132081.
[51] R.S. Ganesh, E. Durgadevi, M. Navaneethan, V. Patil, S. Ponnusamy, C. Muthamizhchelvan, S. Kawasaki, P. Patil, Y. Hayakawa, Tuning the selectivity of NH3 gas sensing response using Cu-doped ZnO nanostructures, Sens. Actuators A 269 (2018) 331–341.
[52] L.J. Kirwan, P.D. Fawell, W. van Bronswijk, In situ FTIR-ATR examination of poly (acrylic acid) adsorbed onto hematite at low pH, Langmuir 19 (2003) 5802–5807.
[53] H. Esgin, Y. Caglar, M. Caglar, Photovoltaic performance and physical characterization of Cu doped ZnO nanopowders as photoanode for DSSC, J. Alloys Compd. 890 (2022) 161848.
[54] S. Thakur, R. Kaur, S.K. Mandal, Size dependence of CdS nanoparticles on the precursor concentration and visible light driven photocatalytic degradation of methylene blue, New J. Chem. 45 (2021) 12227–12235.
[55] D.R. Shinde, P.S. Tambade, M.G. Chaskar, K.M. Gadave, Photocatalytic degradation of dyes in water by analytical reagent grades ZnO, TiO 2 and SnO 2: a comparative study, Drink. Water Eng. Sci. 10 (2017) 109–117.
[56] M. Xu, Y. Chen, W. Hu, Y. Liu, Q. Zhang, H. Yuan, X. Wang, J. Zhang, K. Luo, J. Li, Designed synthesis of microstructure and defect-controlled Cu-doped ZnO–Ag nanoparticles: exploring high-efficiency sunlight-driven photocatalysts, J. Phys. D 53 (2019) 025106.
[57] H. Liu, H. Zhai, C. Hu, J. Yang, Z. Liu, Hydrothermal synthesis of In2O3 nanoparticles hybrid twins hexagonal disk ZnO heterostructures for enhanced photocatalytic activities and stability, Nanoscale Res. Lett. 12 (2017) 1–10.
[58] L. Song, S. Zhang, X. Wu, Q. Wei, A metal-free and graphitic carbon nitride sonocatalyst with high sonocatalytic activity for degradation methylene blue, Chem. Eng. J. 184 (2012) 256–260.
[59] L.V. Devi, S. Sellaiyan, T. Selvalakshmi, H. Zhang, A. Uedono, K. Sivaji, S. Sankar, Synthesis, defect characterization and photocatalytic degradation efficiency of Tb doped CuO nanoparticles, Adv. Powder Technol. 28 (2017) 3026–3038.
[60] M.A. Qamar, S. Shahid, M. Javed, S. Iqbal, M. Sher, M.B. Akbar, Highly efficient g-C3N4/Cr-ZnO nanocomposites with superior photocatalytic and antibacterial activity, J. Photochem. Photobiol. A 401 (2020) 112776.
[61] B. Chen, J. Zhang, J. Yu, B. He, J. Jin, H. Wang, Y. Gong, Rational design of all–solid-state TiO2-x/Cu/ZnO Z-scheme heterojunction via ALD-assistance for enhanced photocatalytic activity, J. Colloid Interface Sci. 607 (2022) 760–768.